Supporting Information

Stem Cell Niche Structure as an Inherent Cause of Undulating Epithelial Morphologies

Jeremy Ovadia and Qing Nie

Center for Mathematical and Computational Biology, Center for Complex Biological Systems, Department of Mathematics, University of California, Irvine, CA, 92697, USA

Corresponding author: Qing Nie (qnie@math.uci.edu)

CONTENTS

I. MECHANISMS TO IMPEDE FINGERING

A. Stem cell niche's regulation of its own cell cycle

The regulation of the longevity and aging of stem cells is important for the aging process for both tissues and organisms since the efficiency of stem cell renewal and the coordination of molecular signaling within a tissue deteriorate over long periods of time (1). Specifically, this regulation must balance the ability for the tissue to regenerate with the potential for cancer and cell overgrowth (2). Recent experimental studies reveal that the stem cell niche plays a critical role in regulating cellular aging in adult stem cells by maintaining stem cells in a quiescent, slow cycling state and modulating gene expression when they are in the niche (3, 4).

In order for the stem cell niche to regulate its own cell cycle lengths, we allow stem cells to secrete a given morphogen M that slows their proliferation rates, ν_0 (see SI.B). Possible candidates to play the role of M could be diffusible members of the Hedgehog signaling family, which have been identified experimentally to assume such a role in the hematopoietic system (5) and also have been strongly linked to basal cell carcinoma (6). Incorporating M into our free-form niche model by inhibiting ν_0 provides us with

$$\frac{\partial M}{\partial t} + \nabla \cdot \left(M\vec{V} \right) = D_M \Delta M + \zeta_0 C_0 - m_{\deg} M, \qquad \nu_0 = \frac{\overline{\nu_0}}{1 + \left(\gamma_M M \right)^k}. \tag{Eq. 1}$$

Here, D_M represents the diffusion coefficient of M; ζ_2 is the rate at which stem cells produce M; $m_{\deg}$ is the degradation rate of M; $\overline{\nu_0}$, $1/\gamma_M$, and k are thresholding, EC50, and hill exponent values for the functional form of ν_0. Imposing the permeability of the basal lamina and the closedness of the apical surface as boundary conditions yields,

$$\left. \frac{\partial M}{\partial y} \right|_{y=0} = 0, \qquad \left. \nabla M \cdot \hat{n} \right|_{y=h} = -\alpha_M M. \tag{Eq. 2}$$

The permeability coefficient for M is given by α_M. Through this construction, M is both secreted only by stem cells in a niche along the basal lamina while also absorbed along the basal lamina. Here, the parameter γ_M corresponds to the strength of the inhibition of M onto ν_0.

Simulations show that when fingers form in a free-form niche while M is secreted to slow the cycling of stem cells, M accumulates along the basal lamina where stem cells are present and is especially high in the fingers of the tissue (Fig. S3A). As a result, the proliferation rate of stem cells is noticeably slowed in these regions, evidenced by lower ν_0 values. Beginning with a spatially varying initial morphology, fingering can be delayed or entirely impeded by the action of M. As γ_M increases, T_h decreases and, when γ_M reaches 45, T_h approaches zero over time (Fig. S3B). Also evident from the simulations is that when the length of the stem cell cycle is increased by M, tissue stratification and overgrowth are delayed while mean tissue size is decreased. For example, when $\gamma_M = 40$, it takes until approximately $t = 100$ for the tissue to reach its largest size, which is more than five times longer than the case in which ν_0 is uninhibited by M. Overall, the stem cell niche's regulation of its own proliferation rates provides one mechanism to delay or prevent morphological distortions of the tissue.

B. Pressure-induced differentiation of stem cells

The external physical environment of a stem cell that the niche provides plays a crucial role in determining cell fates; stem cells often have a multipotency to differentiate in a number of ways as dependent upon their physical environment (7). Recently, signal transduction networks in stem cells, such as the YAP pathway (8), have been shown to play a role in mechanotransduction, the process in which cells biochemically interpret mechanical stimuli. External mechanical stress and pressure from outside the cell provide stimuli to prompt the differentiation of stem cells in vitro (9, 10).

Since internal tissue pressure is accounted for as one of the ways our models capture tissue mechanics, we can study test the effects of pressure-induced differentiation on a multistage cell lineage by allowing the internal tissue pressure to promote stem cell differentiation by inhibiting the stem cell self-replication probability p_0. Due to the fact that the variable describing the pressure, P, assumes both positive and negative values, hill functions are inappropriate to model a feedback response. Instead, we choose to use an arctangent to describe a response in which p_0 is inhibited by both the local concentration of A and the local pressure,

$$p_0 = \frac{\overline{p_0}}{1+\left(\gamma_A A\right)^m}\left[\tfrac{1}{2} - \tfrac{1}{\pi}\arctan\left(\gamma_P P - \zeta_P\right)\right], \qquad \text{(Eq. 3)}$$

Here, γ_P describes the responsiveness of the feedback from P and ζ_P / γ_P is the corresponding EC50 value.

Incorporating pressure-induced differentiation on the fingering of a free-form niche exhibits a general similarity to the hindrance of fingering observed by the stem cell niche's regulation of its own cell cycle times. When the sensitivity of stem cell differentiation to internal

tissue pressure is increased by smaller ζ_P values, T_h attains lower values and mean tissue size is decreased (Fig. S3C). When ζ_P is taken to be small enough (~4), fingering can be prevented entirely, and T_h approaches zero while the tissue size has halved from the case in which pressure has no effect on differentiation.

C. A curvature dependence of the basal lamina's permeability

A key difference between the effects of the stem cell niche slowing its own cell cycle length and pressure-induced differentiation is that the former appears to delay fingering by decreasing the rate of stratification while the latter appears to slow the timescale of the fingering process itself. This conclusion is first apparent in slopes of T_h curves for the pressure-induced differentiation case, which are less steep than the cell cycle regulation case. It is also evident that pressure-induced differentiation prompts earlier stratification and overgrowth, which contrasts with the effects of the inhibition of ν_0 by M, which delay stratification. In both cases, the system does not show evidence of reaching a steady state. We find that a possible mechanism to reach a stable steady state with a distorted free-form niche morphology is to allow the permeability of the basal lamina to depend upon its own curvature (Fig. S4). For this case, stable fingering occurs but with less prominent distortion at a steady state than that comparable to experimentally observed morphological distortions caused by rete pegs and palisades of Vogt.

II. COMPUTATIONAL METHODS

A. Methods for interfacial motion

In order to simulate stem cell tissue models presented here, the growing domain is transformed to the unit square, and interfacial motion is accounted for explicitly (11). We use the following coordinate system on our computational domain

$$\begin{aligned} x &= X, \\ y &= F(X,Y,\tau), \\ t &= \tau, \end{aligned} \qquad \text{(Eq. 4)}$$

where $F(X,1,\tau) = h(x,t)$ and $F(X,0,\tau) = 0$. The transformed derivatives then become

$$\begin{aligned} \frac{\partial}{\partial t} &= \frac{\partial}{\partial \tau} - g_1 \frac{\partial}{\partial Y}, \\ \frac{\partial}{\partial x} &= \frac{\partial}{\partial X} - g_2 \frac{\partial}{\partial Y}, \\ \frac{\partial}{\partial y} &= g_3 \frac{\partial}{\partial Y}, \\ \Delta &= \frac{\partial^2}{\partial x^2} + \frac{\partial^2}{\partial y^2} = \frac{\partial^2}{\partial X^2} + g_4 \frac{\partial^2}{\partial Y^2} + g_5 \frac{\partial^2}{\partial X \partial Y} + g_6 \frac{\partial}{\partial Y}, \end{aligned} \qquad \text{(Eq. 5)}$$

where

$$g_1 = \frac{F_\tau}{F_Y}, \quad g_2 = \frac{F_X}{F_Y}, \quad g_3 = \frac{1}{F_Y},$$

$$g_4 = (g_2)^2 + (g_3)^2, \quad g_5 = -2g_2, \quad g_6 = g_2 \frac{\partial g_2}{\partial Y} + g_3 \frac{\partial g_3}{\partial Y} - \frac{\partial g_2}{\partial X}.$$

Then, the resultant equations are discretized in space using high-order central difference approximations. In particular, fourth-order central difference approximations for the derivatives of h and P in the X-direction are implemented to achieve a necessary accurate treatment of the movement of the boundary due to the presence of second derivatives of h in κ and g_6,

$$\begin{aligned} \frac{\partial f}{\partial X} &\approx \frac{-f_{i+2} + 8f_{i+1} - 8f_{i-1} + f_{i-2}}{12\Delta X}, \\ \frac{\partial^2 f}{\partial X^2} &\approx \frac{f_{i+2} + 16f_{i+1} - 30f_i + 16f_{i-1} - f_{i-2}}{12\Delta X^2}. \end{aligned} \qquad \text{(Eq. 6)}$$

A second-order TVD Runge Kutta is implemented for temporal integration. Discretized forms are solved using multigrid solvers.

B. Simulation details

For spatiotemporal simulations, a 129×129 grid size is implemented for all simulations along with a time-step of $\Delta t = 2 \times 10^{-3}$. Resolution checks were performed on 65×65 and 257×257

grid sizes. Calculations were carried out using FORTRAN 77 with plots generated by MATLAB R2009a (The MathWorks, Natick, MA).

C. Explicit form for the curvature of the dynamic boundary

The curvature, κ, of the tissue's dynamic boundary is given in terms of the derivatives of h by

$$\kappa = \frac{h_{xx}}{\left(1+h_x{}^2\right)^{3/2}}. \qquad \text{(Eq. 7)}$$

D. Definition and computation of stem cell niche size

In this section, we define the size of the stem cell niche, $\sigma(x)$, that forms along the basal lamina in our models for stratified epithelial tissues at a fixed time. First, we define the stem cell niche to be a connected region where the value of C_0 is above $\theta \max\{\min\{C_0(x,0), C_1(x,h)\}\}$ for a given θ between 0 and 1. Next, we define the function Φ for a stratified tissue by

$$\Phi(x) = \max\left\{y : C_0(x,y) \le \theta \cdot \max\left\{\min\left\{C_0(x,0)\right\}, \min\left\{C_0(x,h)\right\}\right\}\right\}. \qquad \text{(Eq. 8)}$$

For a rigid niche, we take $\sigma(x,t) = \Phi(x,t)$ as the size of the stem cell niche. We define the stem cell niche size for the free-form niche by

$$\sigma(x_0) = \left\|\left(x_0, \Phi(x_0)\right) - \left(\bar{x}, h(\bar{x})\right)\right\| \qquad \text{(Eq. 9)}$$

where $\left(\bar{x}, h(\bar{x})\right)$ is the point where the line spanned by the vector normal to Φ at x_0 intersects with h. Specifically, this line is given in slope-intercept form by,

$$y = -\frac{1}{\Phi_x\left(x_0\right)}x + \Phi\left(x_0\right) + \frac{x_0}{\Phi_x\left(x_0\right)}, \qquad \text{(Eq. 10)}$$

and

$$h\left(\bar{x}\right) = \frac{x_0 - \bar{x}}{\Phi_x\left(x_0\right)} + \Phi\left(x_0\right). \qquad \text{(Eq. 11)}$$

Through this definition, the stem cell niche size does not necessarily depend on how many stem cells reside in the tissue but more on how the present stem cells are distributed within the tissue.

To compute $\left(\bar{x}, h(\bar{x})\right)$, let us first assume that our solution $\bar{x}$ is in the interval $\left[x_i, x_{i+1}\right]$ on our computational grid. We can then use linear interpolation to write,

$$\frac{1}{\Delta x}\left[\left(x_{i+1} - \bar{x}^i\right)h_i + \left(\bar{x}^i - x_i\right)h_{i+1}\right] = \frac{x_0 - \bar{x}^i}{\Phi_x\left(x_0\right)} + \Phi\left(x_0\right) \qquad \text{(Eq. 12)}$$

where $h_j = h(x_j)$. Then we can solve for $\bar{x}$ as follows,

$$\bar{x}^i = \frac{x_0 + \Phi\left(x_0\right)\Phi_x\left(x_0\right) + \frac{1}{\Delta x}\Phi_x\left(x_0\right)\left(x_i h_{i+1} - x_{i+1}h_i\right)}{\frac{1}{\Delta x}\Phi_x\left(x_0\right)\left(h_{i+1} - h_i\right) + 1}. \qquad \text{(Eq. 13)}$$

So, to computationally attain $\bar{x}$, one can search through all *i* on the grid to find the unique case when $x_i \le \bar{x}^i \le x_{i+1}$ and take $\bar{x} = \bar{x}^i$. One can use a similar linear interpolation to search on the subintervals of the *y*-grid for a fixed *x* to compute Φ.

III. MATHEMATICAL ANALYSIS OF MORPHOGEN DISTRIBUTION WITH A FREE-FORM NICHE

In this section, we analytically explore how convexity of the basal lamina in a free-form niche may affect the distribution of the morphogen A that is produced in the epithelium and diffuses through the basal lamina.

We begin with the partial differential equation on Ω, describing the quasi-steady state approximation for A,

$$\begin{aligned} 0 &= D_A \Delta A - a_{\deg} A + \sum_{j=0}^{2} \mu_j C_j, \\ \left. \frac{\partial A}{\partial y} \right|_{y=0} &= 0, \\ \nabla A \cdot \hat{n}\big|_{y=h} &= -\alpha_A A, \end{aligned} \tag{Eq. 14}$$

with periodicity in the x-direction and all parameters taken to be positive. By the Divergence Theorem, we have

$$\begin{aligned} \int_\Omega \Delta A dV &= \int_{\partial\Omega} \nabla A \cdot n dV = \\ &= -\alpha_A \int_H A ds, \end{aligned} \tag{Eq. 15}$$

where H is the two-dimensional curve described by h. Substituting for the Laplacian of A yields

$$\alpha_A D_A \int_H A\, ds = \int_\Omega \left(\sum_{j=0}^{2} \mu_j C_j - a_{\deg} A \right) dV. \tag{Eq. 16}$$

Now, let us suppose that all cell types produce A at the same rate, μ, as our computational simulations do. Then

$$\alpha_A D_A \int_H A ds + a_{\deg} \int_\Omega A dV = \mu |\Omega|. \tag{Eq. 17}$$

Assume that h takes the form of a constant perturbed by a sinusoid: $h(x) = \bar{h} + B \sin\left(2\pi k x + \beta\right)$ where $0 \le B \le \bar{h}$. Then $|\Omega|$ is independent of B while

$$|H| = \int_0^1 \sqrt{1 + 4B^2 \pi^2 k^2 \cos^2\left(2\pi k x + \beta\right)} dx \tag{Eq. 18}$$

is increasing with respect to B. Take $B_1 > B_2$ and let Ω_i, H_i, and A_i correspond to choosing B_i for $i = 1, 2$. Thus, we have,

$$\int_{H_1} A_1 ds + \bar{a} \int_{\Omega_1} A_1 dV = \int_{H_2} A_2 ds + \int_{\Omega_2} A_2 dV. \tag{Eq. 19}$$

where $\bar{a} = a_{\deg} / \left(\alpha_A D_A\right)$ and with $|H_1| > |H_2|$.

If $\int_{\Omega_1} A_1\, dV \ge \int_{\Omega_2} A_2\, dV$, then it must follow that $\int_{H_1} A_1\, ds \le \int_{H_2} A_2\, ds$ with $|H_1| > |H_2|$. This indicates that the average value of A_1 over H_1 is less than the average value of A_2 over H_2.

On the other hand, if $\int_{\Omega_1} A_1 \, dV < \int_{\Omega_2} A_2 \, dV$, then we clearly see that the average value of A_1 over Ω_1 is less than the average value of A_2 over Ω_2. So, we can either state that A_1 has a lower average value along the basal lamina than A_2 or that there is less total A in Ω_1 than in Ω_2. This indicates that a greater convexity of the basal lamina may, in some fashion, imply less A either at the base of the tissue or throughout the entire tissue.

IV. PARAMETERS AND INITIAL CONDITIONS USED FOR ALL FIGURES

A. Initial conditions

For speed in reaching a steady state and to prevent rampant overgrowth, we begin simulations with a uniform 10 percent stem cell density and 90 percent TD cell density (i.e. $C_0 = 0.1$, $C_1 = 0$, and $C_2 = 0.9$) along with an initial tissue morphology described by $h(x, t = 0) = 0.1$ unless specified otherwise.

B. Parameters

Unless stated otherwise, the following set of unitless parameters are used for all simulations in Figures 2, 3, 5, and 6:

$$d_2 = 10^{-2} \text{ per cell cycle}$$
$$a_{\text{deg}} = g_{\text{deg}} = m_{\text{deg}} = 10^{-1} \text{ s}^{-1}$$
$$\mu_0 = \mu_1 = \mu_2 = \eta_1 = \eta_2 = \varsigma_0 = 10^{-1} \text{ s}^{-1}\mu\text{M}$$
$$\eta_0 = 0 \ s^{-1}\mu M$$
$$D_A = D_G = 10^{-3} \text{ mm}^2\text{s}^{-1}$$
$$D_M = 10^{-4} \text{ mm}^2\text{s}^{-1}$$
$$\alpha_A = \alpha_G = 10 \text{ mm}^{-1}$$
$$\gamma_A = 1.1 \text{ } \mu\text{M}^{-1}$$
$$\gamma_G = 5 \text{ } \mu\text{M}^{-1}$$
$$\gamma_P = 30 \text{ } \mu\text{M}^{-1}$$
$$\bar{p}_0 = 0.7, \bar{p}_1 = 0.4,$$
$$\nu_0 = \bar{\nu}_0 = \nu_1 = 1 \text{ per cell cycle}$$
$$\xi = 4 \times 10^{-3}, K = 10^{-3}$$

which are very similar to those used in (12).

The following set of parameters is used for Figure 4:

$$d_2 = 0.2 \text{ per cell cycle}$$
$$a_{\text{deg}} = g_{\text{deg}} = 0.2 \text{ s}^{-1}$$
$$\mu_0 = \mu_1 = \mu_2 = \eta_1 = \eta_2 = 1 \text{ s}^{-1}\mu\text{M}$$
$$\eta_0 = 0 \ s^{-1}\mu M$$
$$D_A = D_G = 10^{-2} \text{ mm}^2\text{s}^{-1}$$
$$\alpha_A = \alpha_G = 10^2 \text{ mm}^{-1}$$

$$\gamma_A = 3 \ \mu\text{M}^{-1}$$
$$\gamma_G = 2 \ \mu\text{M}^{-1}$$
$$\bar{p}_0 = 0.75, \bar{p}_1 = 0.45,$$
$$\nu_0 = \nu_1 = 1 \text{ per cell cycle}$$
$$\xi = 5 \times 10^{-3}, K = 10^{-3}$$

All hill exponents are taken to be 2 throughout all simulations.

C. Further explanation of tissue movement at the fixed boundary

The boundary condition for $\frac{\partial P}{\partial y}(x, y = 0, t) = 0$ at the fixed boundary $y = 0$ requires that the vertical component of the tissue velocity there is zero, $w(x, y = 0, t) = 0$. However, there is no restriction of the horizontal movement of the tissue along this boundary, meaning no restriction is placed on u at this boundary. This boundary condition differs from a "no-slip" boundary condition in which both u and w would be required to be zero at the boundary $y = 0$.

The models presented here allow for horizontal movement along the fixed boundary since there is often spatially nonuniform influx and outflux along this boundary. In some rigid niche simulations (Fig. 2A-D for example), stem cells and TA cells self-renew more often along the basal lamina where the basal lamina is more permeable. At the same time, TD cells may also be more populous along some regions of the basal lamina than others, causing a spatially nonuniform cell death rate there. Thus, as a result, the influx and outflux of cells varies spatially along the basal lamina for the rigid niche, which would result in cell movement in the horizontal direction along the basal lamina. So, the boundary condition of no vertical movement along $y = 0$ without imposing a no-slip boundary maintains the geometry of the tissue while enabling necessary cell movement in the horizontal direction.

D. Perturbations for figures from main text

An initial perturbation to tissue morphology for Figure 2:

$$h(x,t=0) = 0.1\big(1+0.25\cos(4\pi x)\big)$$

$$T_h(t=0) = 0.4$$

A spatial perturbation to the permeability of the basal lamina for Figure 2:

$$\alpha_A(x) = \bar{\alpha}_A(1+0.25\cos(4\pi x)), \quad \alpha_G(x) = \bar{\alpha}_G(1+0.25\cos(4\pi x))$$

An initial perturbation to tissue morphology for Figure 3:

$$h(x,t=0) = 0.1\big(1+0.025\cos(4\pi x)\big)$$

$$T_h(t=0) \approx 0.0488$$

An initial perturbation to tissue morphology for Figure 4:

$$h(x,t=0) = 0.1\big(1+0.025\cos(2k\pi x)\big)$$

$$T_h(t=0) \approx 0.0488$$

An initial perturbation to tissue morphology for Figure 5:

$$h(x,t=0) = 0.1\big(1+0.025\cos(2k\pi x)\big)$$

$$T_h(t=0) \approx 0.0488$$

Distinct spatial perturbations to components of the cell lineage for Figure 5:

$$p_0(x) = \overline{p_0}(1+0.025\cos(4\pi x)),$$

$$p_1(x) = \overline{p_1}(1+0.025\cos(4\pi x)),$$

$$\nu_0(x) = \overline{\nu_0}(1+0.025\cos(4\pi x)),$$

$$\nu_1(x) = \overline{\nu_1}(1+0.025\cos(4\pi x)),$$

$$d_2(x) = \overline{d_2}(1+0.025\cos(4\pi x))$$

A spatial perturbation to the permeability of the basal lamina for Figure 5:

$$\alpha_A(x) = \bar{\alpha}_A(1+0.025\cos(4\pi x)), \quad \alpha_G(x) = \bar{\alpha}_G(1+0.025\cos(4\pi x))$$

An initial perturbation to tissue morphology for Figure 6:

$$h(x,t=0) = 0.1\big(1+0.025\cos(4\pi x)\big)$$

$$T_h(t=0) \approx 0.0488$$

V. SUPPORTING REFERENCES

1. Silva, H., and I. M. Conboy. 2008. Aging and stem cell renewal. StemBook:1-14.
2. Orford, K. W., and D. T. Scadden. 2008. Deconstructing stem cell self-renewal: genetic insights into cell-cycle regulation. Nature Reviews Genetics 9:115-128.
3. Wagner, W., P. Horn, S. Bork, and A. D. Ho. 2008. Aging of hematopoietic stem cells is regulated by the stem cell niche. Experimental Gerontology 43:974-980.
4. Gopinath, S. D., and T. A. Rando. 2008. Stem cell review series: aging of the skeletal muscle stem cell niche. Aging Cell 7:590-598.
5. Trowbridge, J. J., M. P. Scott, and M. Bhatia. 2006. Hedgehog modulates cell cycle regulators in stem cells to control hematopoietic regeneration. Proceedings of the National Academy of Sciences of the United States of America 103:14134-14139.
6. Daya-Grosjean, L., and S. Couve-Privat. 2005. Sonic hedgehog signaling in basal cell carcinomas. Cancer Letters 225:181 - 192.
7. Cohen, D. M., and C. S. Chen. 2008. Mechanical control of stem cell differentiation. StemBook:1-16.
8. Dupont, S., L. Morsut, M. Aragona, E. Enzo, S. Giulitti, M. Cordenonsi, F. Zanconato, J. Le Digabel, M. Forcato, S. Bicciato, N. Elvassore, and S. Piccolo. 2011. Role of YAP/TAZ in mechanotransduction. Nature 474:179-183.
9. Altman, G. H., R. L. Horan, I. Martin, J. Farhadi, P. R. H. Stark, V. Volloch, J. C. Richmond, G. Vunjak-Novakovic, and D. L. Kaplan. 2001. Cell differentiation by mechanical stress. The FASEB Journal 16:270-272.
10. Lee, I. C., J. H. Wang, Y. T. Lee, and T. H. Young. 2007. The differentiation of mesenchymal stem cells by mechanical stress or/and co-culture system. Biochemical and Biophysical Research Communications 352:147-152.
11. Wang, J., and G. Baker. 2009. A numerical algorithm for viscous incompressible interfacial flows. J. Comput. Phys. 228:5470-5489.
12. Chou, C.-S., W.-C. Lo, K. K. Gokoffski, Y.-T. Zhang, F. Y. M. Wan, A. D. Lander, A. L. Calof, and Q. Nie. 2010. Spatial Dynamics of Multi-stage Cell-Lineages in Tissue Stratification. Biophysical Journal 99:3145-3154.

VI. SUPPORTING FIGURES

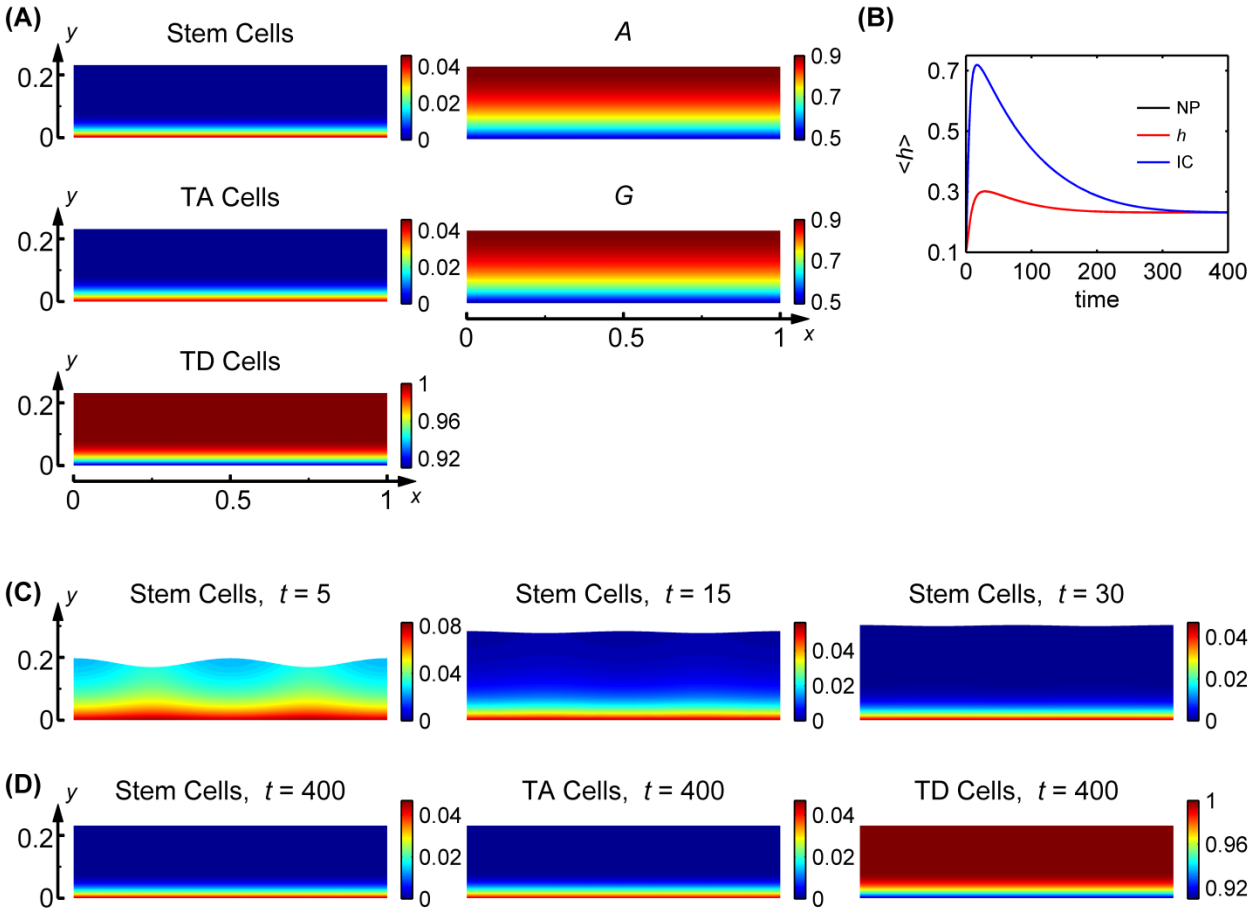

FIGURE S1: A uniform, homeostatic steady state with a rigid niche. (A) Approximate steady state distributions for stem, TA, TD cells, and the regulatory molecules A and G for rigid niche simulation with homogeneity in the x-direction. (B) Mean tissue size over time for three cases: 1) homogeneity in the x-direction with no spatial perturbations (*NP*) ; (2) an initial perturbation to tissue morphology $h(x,0) = 1 + 0.25\cos(4\pi x)$; and (3) an initial condition of cell distributions given by $C_0(x,y,t=0) = 0.25(1+\cos(4\pi x)\cos(4\pi y/h))$, $C_1(x,y,t=0) = 0.25(1+\sin(4\pi x)\sin(4\pi y/h))$, and $C_2(x,y,t=0) = 1 - C_0(x,y,0) - C_1(x,y,0)$. Simulations for three cases appear to approach the same steady state. (C) Dynamics of the distribution of stem cells for case 2. (D) Approximate steady state cell volume fraction distributions for case 2.

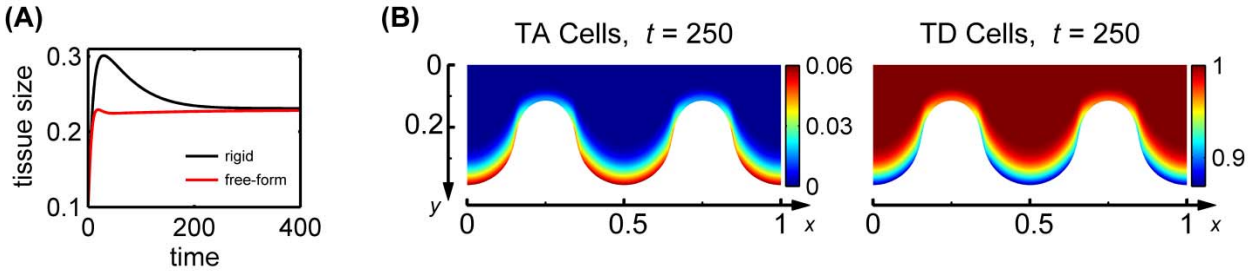

FIGURE S2: Dynamics of the free-form niche. (A) Mean tissue sizes for rigid and free-form stem cell niches with spatial homogeneity in the x-direction. (B) Distributions of TA and TD cell volume fractions in a distorted tissue morphology at time $t = 250$.

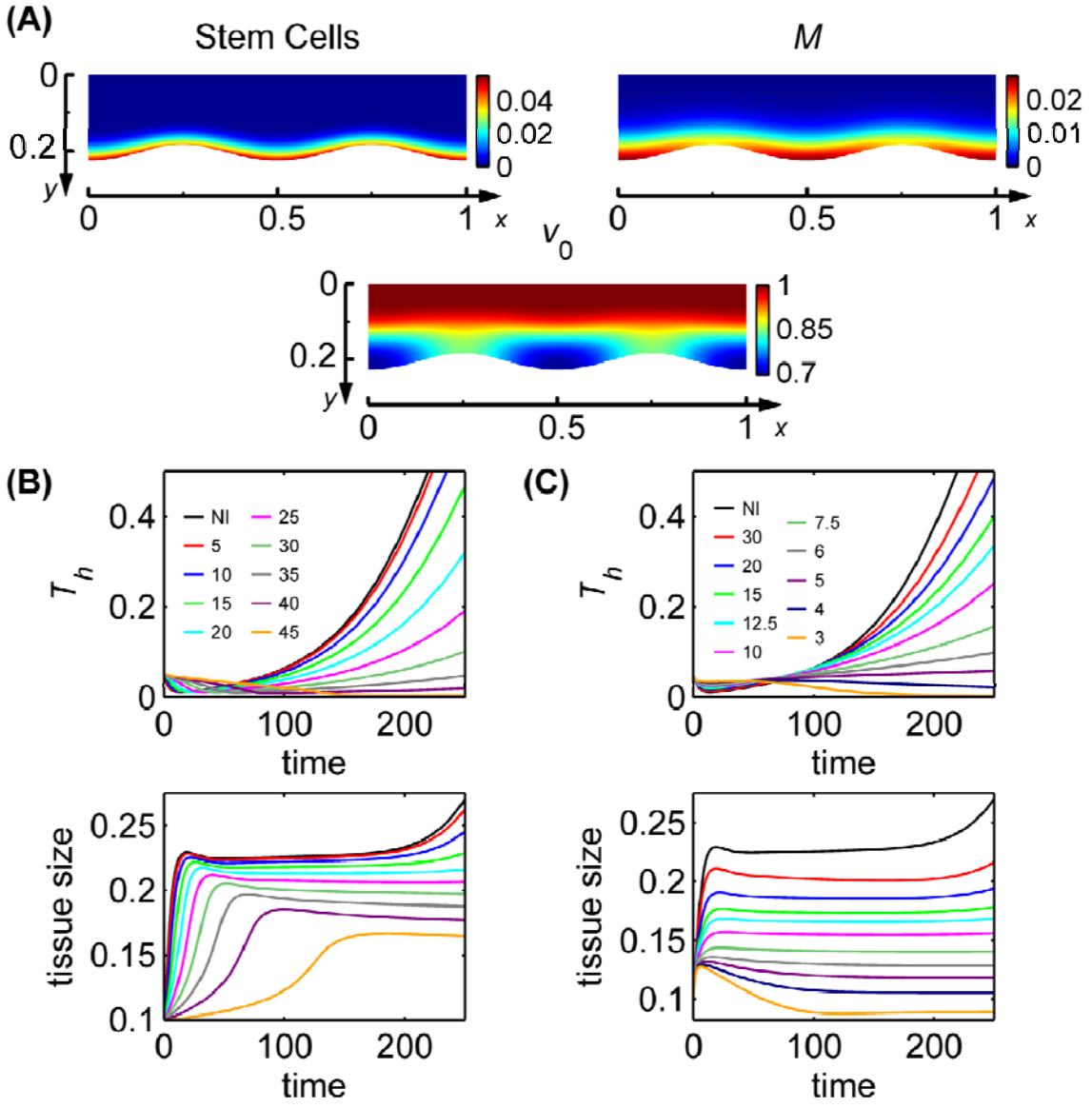

FIGURE S3: The stem cell niche's regulation of its own cell cycle times and pressure-induced differentiation of stem cells can impede distortion of epithelial morphologies with a free-form niche. Simulation details are listed in SIV. (A-B) Simulations incorporating the inhibition of the proliferation rate v_0 by the diffusible molecule M produced by stem cells. (A) Distributions of stem cells, M, and v_0 at time $t = 250$ for $\gamma_M = 20\,\mu\text{M}^{-1}$. (B) Variation in tissue size, T_h, and mean tissue size over time for varying γ_M-values. (C) Variation in tissue size, T_h, and mean tissue size over time for simulations incorporating the inhibition of the replication probability p_0 by the local internal pressure with varying ζ_P-values. 'NI' denotes cases with no inhibition.

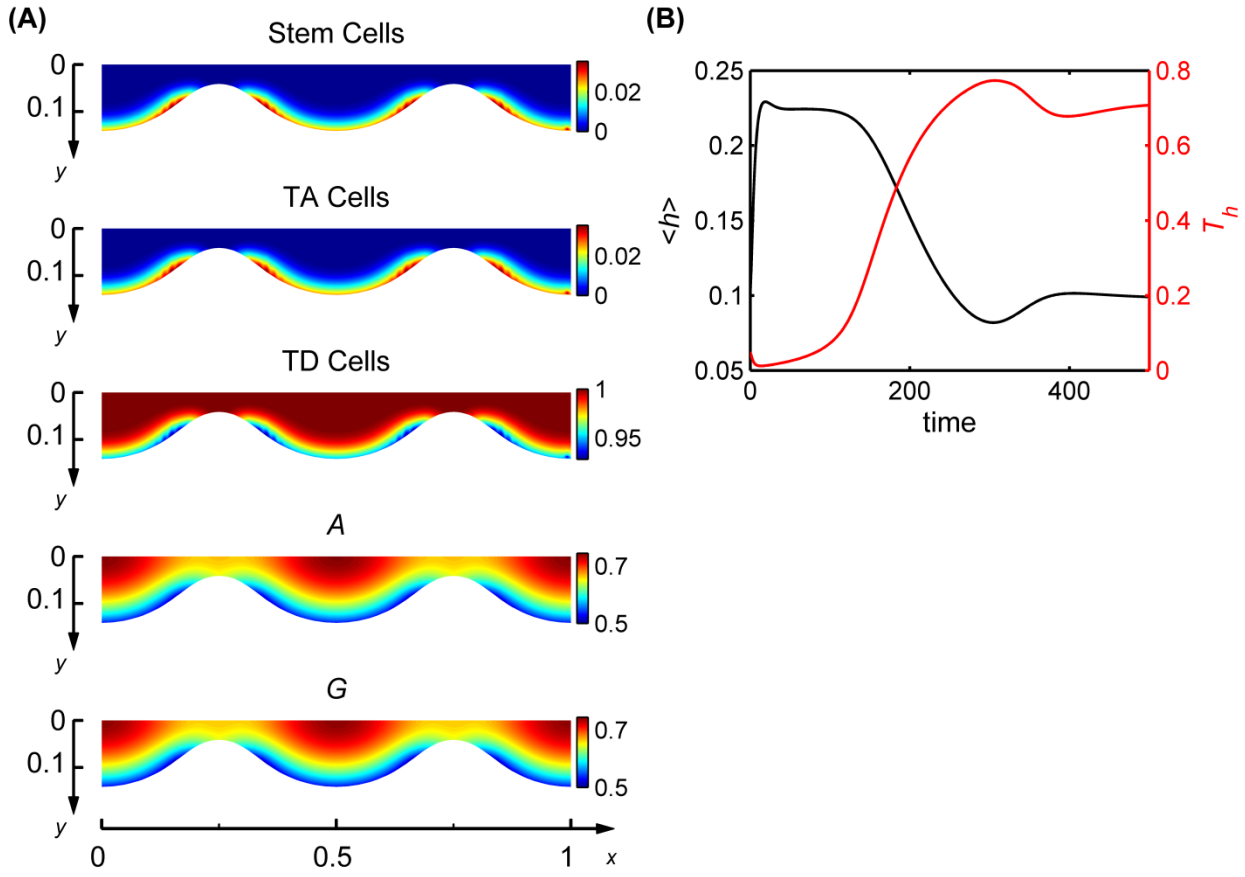

FIGURE S4: Stabilizing an undulated morphology by a curvature dependence of the basal lamina's permeability Simulation details are listed in SIV. The initial tissue morphology is described by $h(x,0) = 1 + 0.25\cos(4\pi x)$ with a free-form niche. The permeability of the basal lamina is assumed to take the form $\alpha_A(x) = \bar{\alpha}_A / (1 + (50\xi\kappa)^2)$. (A) Cell and regulatory molecule distributions at time $t = 400$. (B) Temporal dynamics of mean tissue size, $< h >$, and variation in tissue size, T_h.